Astronomy & Astrophysics manuscript no. Conn287
February 21, 2022
© ESO 2022

arXiv:1906.09782v1 [astro-ph.HE] 24 Jun 2019

Connection between optical and radio/millimeter flares in blazar OJ287

S.J. Qian[1]

National Astronomical Observatories, Chinese Academy of Sciences, Beijing 100012, China

Complied by using A&A latex

ABSTRACT

Context. Blazar OJ287 is a unique source in which optical outbursts with double-peak structure have been observed quasi-periodically with a cycle of ∼12 yr. It may be one of the best candidates for searching supermassive black hole binaries.
Aims. We investigate the connection between its optical and radio/millimeter variations and interpret the emissions in terms of relativistic jet models.
Methods. Specifically, we make a detailed analysis and model simulation of the optical and radio/mm light curves for the outburst during the period of 1995.8–1996.1.
Results. It is shown that the multi-wavelength light-curves at optical V-band and radio/mm wavelengths (37, 22, 14.5 and 8 GHz) can be decomposed into 36 individual elementary flares, each of which have symmetric profiles.
Conclusions. The elementary flares can be understood to be produced through lighthouse effect due to the helical motion of corresponding superluminal optical/radio knots. Helical motion of superluminal knots should be prevailing in the inner regions of its relativistic jet formed in the magnetosphere of the putative supermassive black hole/accretion disk system. A comprehensive and compatible framework for understanding the entire phenomena in OJ287 is described.

Key words. galaxies: active – galaxies: jets – galaxies: nuclei – galaxies : individual OJ287

1. Introduction

OJ287 (z=0.306) is one of the best studied and most prominent blazars. It has shown large amplitude and rapid variability at all wavelengths from radio, optical through to γ-rays with various time-scales from hours to years. A large amount of observations in radio, infrared, optical, ultraviolet, X-rays and γ-rays have been carried out to investigate the nature of the phenomena in this source (e.g., Usher 1979, Holmes et al. 1984, Brown et al. 1989, Hartman et al. 1999, Sillanpää et al. 1988, 1996a, 1996b, Takalo 1996a, Takalo et al. 1996b, Allen et al. 1982, Aller et al. 1994, 2014, Tateyama et al. 1999, Valtaoja et al. 2000, Qian 2018, Britzen et al. 2018, Hodgson et al. 2017, Valtonen et al. 2017, Cohen 2017, Kushwaha et al. 2018a, 2018b, Gupta et al. 2016, Agudo et al. 2012, Ackermann et al. 2011, Neronov & Vovk 2011).
With the distinct properties common for generic blazars, the most remarkable characteristic of OJ287 is the quasi-periodic variability in optical wavebands. The optical light curve recorded since 1890s reveals quasi-periodic outbursts with a cycle of ∼12 yr (Sillanpää et al. 1988). Up to now four quasi-periodic outbursts with double-peak structure have been observed in 1971–73, 1983–84, 1994–95 and 2005–2007. The first flare of the fifth quasi-periodic outburst was observed in December 2015 and the second one has been predicted to appear soon (Valtonen et al. 2018, Dey et al. 2018).
The quasi-periodicity in the optical outbursts and their double structure are widely believed to be related to the orbital motion of the putative black hole binary in its nucleus. The very complex variations in flux density and polarization at all wavelengths from radio to γ-rays are mostly believed to occur in the relativistic jet of the primary hole (or both jets produced by the primary and secondary holes; Qian 2018). Various theoretical models (or scenarios) have been proposed to interpret the whole phenomena observed in OJ287 (for details, referring to the discussions in Villforth et al. 2010 and Qian 2018, 2015). On the whole, these models can be divided into two categories: disk-impact models and relativistic jet models, both involving a supermassive black hole binary in the nucleus of OJ287.

– The disk-impact model originally proposed by Lehto & Valtonen (1996) has been steadily improved (Valtonen 2007, Valtonen et al. 2006, 2018, Dey et al. 2018) to interpret the double-peak structure of the quasi-periodic optical outbursts. It suggests that the first major flares of the quasi-periodic outbursts are produced by the secondary hole penetrating into the accretion disk of the primary hole and are thus bremsstrahlung in origin. In the case of highly eccentric orbital motion with large inclination, two impacts would occur per pericenter passage, causing the double-peak structure. The follow-up flares, as well as the non-periodic outbursts occurred during the intervening periods are suggested to be related to the enhanced accretion events induced by the disk-impacts and tidal interaction between the secondary hole and the primary disk. This model requires a high inclination angle (i ∼50° – 90°) and a large orbit eccentricity (e ∼ 0.66) and a strong constraint on the total mass of the binary, reaching $\sim 2\times10^{10} M_{\odot}$ with a mass ratio m/M∼0.007. This model has been elabo-

rated to make accurate timing of the quasi-periodic outbursts.
The cavity-accretion flare model proposed by Tanaka (2013) is another type of disk-impact model, which assumes that the primary hole and the secondary hole having comparable masses and are in near-coplanar orbital motion. Hydrodynamic/magnetohydrodynamic (HD/MHD) simulations for such binaries surrounded by circumbinary disks have shown that cavity-accretion processes would create two gas-flow streams impacting onto the disks of the black holes per pericenter passages, possibly causing the double-peak structure of the quasi-periodic outbursts. This model also suggest that the gas-flow impacts produce thermal outbursts, but it is not able to make accurate timing of the quasi-periodic outbursts. The follow-up flares and the non-periodic outbursts during the intervening periods were not investigated in this model.

– It is widely suggested that blazars are extragalactic sources with relativistic jets pointing close to our line of sight, and they are the brightest and most violently variable active galactic nuclei in radio, optical through to γ-rays. Relativistic jet models have been applied to interpret the optical and radio variability behavior in OJ287 by many authors (e.g., Sillanpää et al. 1996a, Valtaoja et al. 2000, Villata et al. 1998, Villforth et al. 2010, Britzen et al. 2018, Qian 2015, 2018).
Recently, Qian (2019) has tentatively proposed an alternative jet model to understand the entire phenomena in OJ287, which is based on the optical multi-wavelength and γ-ray observations performed for OJ287 (e.g., Kushwaha et el. 2018a, 2018b), combining with the distinct features previously found in the optical and radio (flux and polarization) variations (e.g, Sillanpää et al. 1996a, Valtaoja et al. 2000, Usher 1979, Holmes et al. 1984, Kikuchi et al. 1988, D'Arcangelo et al. 2009, Kushwaha et al. 2018a, Britzen et al. 2018, Qian 2018). The main emission properties are explained, including the following aspects (for details, referring to Qian 2019). (1) The γ-ray flare observed in December/2015 was observed to be closely associated with the optical outburst. The simultaneity between the optical and γ-ray flares implies that the optical outburst in December/2015 (peaking at 2015.92) should be produced in the jet and a nonthermal (synchrotron) flare; (2) The optical multi-wavelength observations (Kushwaha et al. 2018a) have shown that the December/2015 optical outburst has its temporal and spectral variability behavior very similar to that of the synchrotron outburst in March/2016. The two outbursts form a pair of flaring events with a time-interval of $\sim$90 days. Thus the December/2015 outburst must be a synchrotron flare and can not be a thermal flare as claimed in the disk-impact model; (3) Previous observations have already shown that the major optical outbursts can be decomposed into a number of elementary flares, each having a symmetric flux density profile. Symmetry in the light-curves has been recognized as a distinct feature of the optical flares in OJ287; (4) The simultaneous variations in radio/mm and optical bands without measurable time-delays (<1-2 days) and the similarity between the envelopes of optical and radio/mm outbursts imply that these correlations can only be interpreted in terms of lighthouse effect due to the helical motion of superluminal optical/radio knots; (5) Under the lighthouse scenario the December/2015 and the March/2016 outbursts can be interpreted as produced when the superluminal knot (shock) propagates along the helical magnetic field in a perfect-collimation zone through two revolutions.

As shown in Qian (2019) The light-curves of six quasi-periodic optical outbursts (in 1983.0, 1984.1, 1994.8, 2005.8, 2007.7 and 2015.9) and a few individual non-periodic outbursts (in 1993.9, 1994.2 and 2016.98) have been model-simulated and well interpreted in terms of the lighthouse model. We suggest that all these outbursts are synchrotron flares produced in the relativistic jet.
While this relativistic jet model can well explain the light-curves of both the periodic and non-periodic outbursts,[1] it needs to invoke the dual-stream flow accretion mechanism to interpret the double-structure of the quasi-periodic outbursts as in the cavity-accretion flare model by Tanaka (2013). In principle, this is possible as some MHD simulations have demonstrated (e.g., Artymovicz & Lubow 1996, Artymoviz 1998, Hayasaki et al. 2008, Shi et al. 2012, D'Orazio et al. 2013), but detailed modeling is imperatively required, especially for the timing of the optical outbursts (the $\sim$12 yr quasi-periodicity and the $\sim$1-2 yr time-separation of the double-peak structure). Simulations of the accretion events causing all the outbursts during the whole 12 yr period (or even during the 120 yr period) may be also important.
We point out that the relativistic jet models distinguish from the disk-impact models mainly in two aspects.
(1) In the relativistic jet models all the optical outbursts (both quasi-periodic and non-periodic) originate from synchrotron process and thus are related to its primary-hole jet (or to both jets of the primary and secondary holes, Qian 2018). In the disk-impact models the primary quasi-periodic optical outbursts are assumed to originate from bremsstrahlung process due to the secondary hole impacting onto the primary-hole disk, while the follow-up and non-periodic outbursts are assumed to originate from synchrotron process, related to its primary hole jet.
(2) Therefore, in the relativistic jet models, the energetics of the optical outbursts is physically unified: the time-scale of all the optical outbursts is compressed and their flux density boosted by Doppler effects in the same way. The light-curve of all the optical outbursts can be considered in a unified physical frame. In contrast, the disk-impact models require dual-energetics : the synchrotron outbursts are Doppler boosted while the impact (thermal) outbursts are not. This implies that one needs different scales (both time-scale and flux density scale) to describe their energy content and scaling of light-curve for the two types of outbursts. For example, a synchrotron optical flare could have been Doppler boosted by a factor of $\sim 10^5$ (see Section 3), corresponding to a brightness magnification of $\sim$12.5 mag, while the impact flares are not Doppler-boosted.
In this paper we will investigate the simultaneous radio/millimeter and optical variations occurred in OJ287 and provide more evidence for the validity of the lighthouse scenario proposed in Qian (2019).

[1] Relativistic jet models are usually applied to explain the flaring properties in generic blazars from radio, optical (flux and polarization) through to γ-rays.

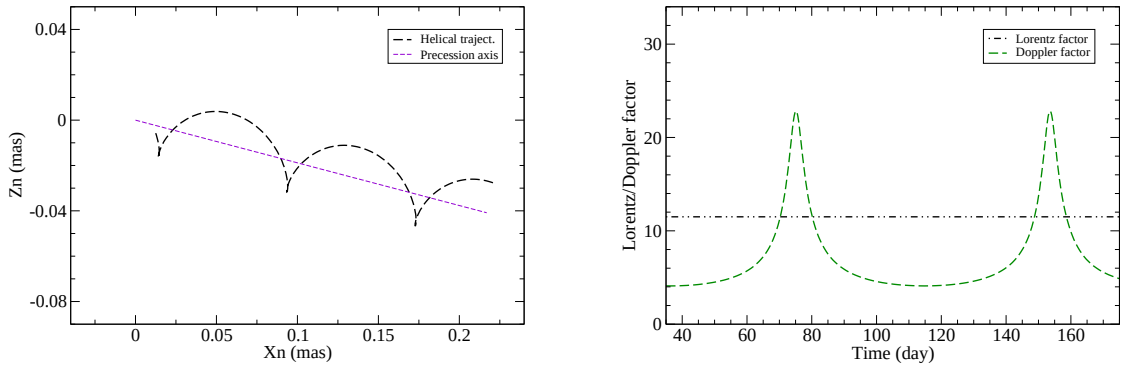


Fig. 1. Left panel: Scenario for a precessing jet and helical motion. The straight line denotes the precessing jet axis (projected on the plane of the sky) which is defined by precession phase ω=–2.0 rad. The helix indicates the trajectory of the optical knot moving around the jet axis in the perfect collimation zone for the elementary flare in 1995.98 (peaking at JD2450075). The corresponding Lorentz and Doppler factors are shown in the right panel.

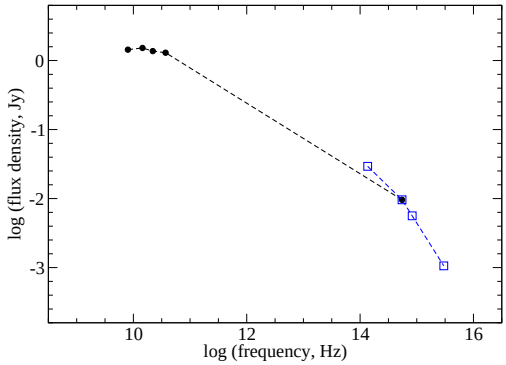


Fig. 2. Modeled spectrum of the elementary optical/radio flare in 1995.98 (peaking at JD2450075; filled black circles). In order to simulate the radio light-curve the spectral indexes between the optical and radio frequencies are selected to be: $\alpha_{37,\rm v}\equiv\alpha$(37GHz,V-band)=0.51, $\alpha_{22,\rm v}\equiv\alpha$(22GHz,V-band)=0.49, $\alpha_{15,\rm v}\equiv\alpha$(14.5GHz,V-band)=0.48 and $\alpha_{8,\rm v}\equiv\alpha$(8GHz,V-band)=0.45, respectively. The K-, U- and UV-band flux densities (open squares) are displayed for comparison. No data are available for the wavelengths between 37 GHz and V-band and the dashed line is only as an aid to the eye.

Table 1. Parameters defining the precessing jet-nozzle scenario and the helical trajectory of the superluminal knot, which are used in the model simulation of the optical and radio light-curves.

Parameter	fixed value
ϵ	3°
ψ	0.0 rad
ω	–2.0 rad
a	0.0402
x	1.0
A_0	0.0138 mas
$\mathrm{d}\phi/\mathrm{d}z_0$	-7.04 rad/mas

Table 2. Base-level (or underlying jet) spectrum selected for the 1995.84 optical and radio/mm outbursts.

Waveband	Flux density
37 GHz	2.31 Jy
22 GHz	2.31 Jy
14.5 GHz	1.30 Jy
8 GHZ	1.30 Jy
V-band	2.70 mJy

2. Basic considerations

The variability behavior of blazar OJ287 is very complex. In order to understand the entire phenomena observed in this blazar, a detailed summary analysis of its flaring characteristics observed at radio, infrared, optical wavelengths and in γ-rays have been made in Qian (2019), including: (1) simultaneous optical and γ-ray flares; (2) spectral energy distribution of the outbursts; (3) similarity in temporal and spectral variations of quasi-periodic outbursts and non-periodic (synchrotron) outbursts; (4) simultaneity in radio/millimeter and optical variations; (5) color stability during the NIR-optical-UV outbursts (for both quasi-

Table 3. Modeled spectrum between 8 GHz and V-band of the simultaneous radio-optical flare observed in 1995.98 (peaking at JD2450075). The K-, U- and UV-band flux densities are given for comparison. They are derived from the modeled V-band flux density, assuming a broken power-law spectrum at the infrared-optical-UV wavelengths with the spectral index changing from 0.8 to 1.3 at the V-band break (Qian 2019, Kushwaha et al. 2018a).

Waveband	Flux density
37 GHz	1.30 Jy
22 GHz	1.37 Jy
14.5 GHz	1.52 Jy
8 GHz	1.44 Jy
K-band	29.3 mJy
V-band	9.59 mJy
U-band	5.62 mJy
UV-band	1.06 mJy

Table 4. Modeled comoving (or de-boosted) flux densities for the elementary flare in 1995.98 (peaking at JD2450075). Numbers in the parentheses represent the powers of ten.

Waveband	Flux density
37 GHz	4.79(-6) Jy
22 GHz	5.05(-6) Jy
14.5 GHz	5.61(-6) Jy
8 GHz	5.31(-6) Jy
V-band	3.53(-5) mJy

periodic and non-periodic) ; (6) broken power-law spectra in NIR-optical-UV bands, (7) decomposition of light-curves of optical outbursts into elementary flares; (8) symmetry in the profiles of optical outbursts; (9) possible existence of double jets produced by the putative black hole binary system; (10) connection between the optical outbursts and the emergence of superluminal radio knots; (11) distinctive variations in optical and radio polarization; (12) similarity in light-curve structure of the quasi-periodic outbursts (e.g. Sillanpää et al. 1985); (13) association of low polarization degree with rapid polarization angle change in quasi-periodic optical outbursts (e.g., Villforth et al. 2010); etc.
Based on the summarization of all these characteristics, the precessing jet nozzle model previously proposed by Qian et al. (1991, 2017, 2018) has been used to simulate the light-curves of the quasi-periodic outbursts in 1983.00, 1984.10, 1994.75, 2005.76, 2007.70, 2015.75 and a few non-periodic flares. It has shown that both periodic and non-periodic optical outbursts may be synchrotron flares originated from the relativistic jet. Their light curves can be interpreted in terms of lighthouse effect due to the helical motion of the superluminal optical knots.
Here we would like to mention some results of the investigations obtained in earlier years as supplementary arguments for the synchrotron origin of the quasi-periodic optical outbursts in OJ287.

– Usher (1979) studied the multi-frequency light-curves of the outburst observed in OJ287 during the period of 1971–1975 [2] and suggested that there is a multi-frequency optical-radio synchrony within observational uncertainty for bursts III, IV and V (as called in that paper), which peaked at ∼1973.0, 1973.9 and 1975.1 respectively. Burst II (peaking at ∼1971.7) could be also synchronous at optical and radio wavelengths, if it is the result of superposition of two or more bursts. It is noted that optical bursts II and III (the strongest and secondary strong flares in this outburst event) have been identified as the double "impact (thermal) flares" of the quasi-periodic outburst (Dey et al. 2018). Thus the radio variations synchronous with the optical variations observed for bursts II and III may imply that the optical outbursts are nonthermal (synchrotron) flares. In this paper we will investigate the correlation between the optical and radio variability observed in the quasi-periodic outburst during 1995.8–1996.1 in OJ287 and further show that the radio variations simultaneous with the optical variations indicate that this optical outburst is nonthermal.

– Holmes et al. (1984) made simultaneous observations of OJ287 at infrared JHK wavelengths and in optical and near infrared wavelengths at UBVRI in 1983 January (during 4 days from January 7 to January 10). This time-interval just coincided with the peaking stage of the primary quasi-periodic outburst (Valtaoja et al. 2000), which was identified as an "impact (thermal) burst" in the precessing binary model (Lehto & Valtonen 1996, Sundelius et al. 1997, Valtonen et al 2018, Dey et al. 2018).[3] The very low polarization degrees of p<1% at R- and V-bands observed on January 8 (a dip in the polarization curves) were regarded as the rational evidence for the optical outburst being a thermal flare. However, the rapid daily variations in polarization angle at R-band (∼ 60°) and V-band (∼ 110°) during one-day period (from January 8 to January 9)[4] does not support this interpretation, because appearance of a thermal outburst (with zero polarization) can greatly reduce the polarization degree of the source, but can not cause its variations in polarization angle. This argument seems important: occurrence of very low polarization degrees (<2-4%) alone cannot be simply recognized as a sign of strong thermal outburst appearing, because the associated variations in polarization angle must be due to synchrotron components.
In order to interpret the simultaneous multi-wavelength light-curves of time-variable flux density S(ν,t), polarization degree p(ν,t) and polarization angle PA(ν,t) in K-, H-, J-, I-, R-, V-, B-, and U-bands, Holmes et al. proposed a two-component model (also see Björnsson 1982, Björnsson & Blumenthal 1982, Königl & Choudhuri 1985 for jet polarization models). [5] They strongly sug-

[2] The light-curves were compiled from the data published in literature at wavelengths of 0.44μm, 10μm, 0.35, 0.9, 2.8, 3.8, 4.5, 6, 11, and 18 cm.

[3] The starting epoch of the 1983.0 outburst (1982.964) has been taken as a standard reference-epoch for the outburst timing in all versions of the disk-impact model (Lehto & Valtonen 1996, Sundelius et al. 1997, Valtonen et al. 2018).

[4] Similar polarization behavior was observed at B-band and U-band.

[5] It should be noted that this model seems to be one of the most effective jet models to coherently explain the complete

gested that the two components are physically connected with one component having a stable polarization angle while the other one showing a gradual rotation. This behavior may be understood in terms of a physical rotation of the magnetic field. Obviously, their modeling results are consistent with the helical motion model (lighthouse model) proposed in Qian (2019) and the two model-components might be related to the jets produced by the primary and secondary black holes, respectively (Qian 2018). In addition, Kikuchi et al. (1988) observed a synchronous rapid variations of polarization angles during February 3–12 1986 in the optical and radio wavebands on time-scale of days. They explained this correlated variation in terms of a shock of "core-envelope" structure moving along the helical magnetic field in the jet. Moreover, the 1983.0 outburst has spectral curvatures in infrared-optical and optical-ultraviolet regions with concave or convex structures which can be also explained in terms of the two-component model together with the polarization features. It seems that the distinct spectral structures observed for the 2015 quasi-periodic outburst in IR-optical-UV wavebands (Kushwaha et al. 2018a) could be interpreted in terms of a jet model like that proposed by Holmes et al. (1984).

We further point out that very low polarization degrees were observed in the quasi-periodic optical outbursts in September 2007 (Villforth et al. 2010) and December 2015 (Valtonen et al. 2017). In both cases the associated rapid variations in polarization angle may indicate that the optical outbursts are nonthermal flares produced in the relativistic jet. The time-variable polarization degree curve should be interpreted coherently with the interpretation of the time-variable flux density curve and polarization angle curve.

– D'Arcangelo et al. (2009) explored the correlation between polarization characteristics at optical and near-infrared (NIR) wavelengths and that in the 43 GHz compact core in OJ287 between 2005 October 24 and November 3 and between 2006 March 27 and April 4. They found that during this period the polarization degrees in the optical, near-infrared and radio-core are nearly steady. They measured the mean R-band polarization degree to be 30.7% which appears to oscillate with a period of ~ 2 days. Interestingly, the polarization degrees in B-, V-, R- and I-bands have similar values and synchronous variations. D'Arcangelo et al. fit the optical spectra with a power-law and found an steady optical spectral index of $\sim$1.28$\pm$0.05. We notice that the first (strongest) flare of the quasi-periodic optical outburst in 2005.74, which was identified as a thermal impact-flare in the precessing binary model (Valtonen & Ciprini 2011), peaked between 2005 October 17 and October 28. Thus the high polarization degrees ($\sim$30%) observed at multi-wavelengths (B-, V-, R- and I-wavebands) by D'Arcangelo et al. between October 25 and 28 should be ascribed to this optical flare, demonstrating its origin of synchrotron radiation. The short rotation (from 20° to 8°) measured between 2005 October 25 and October 29 also favors relativistic jet models (Qian 2019).

Moreover, D'Arcangelo et al. suggested that the variable optical-NIR emission observed during the two campaigns in 2005 and 2006 originates from the 43 GHz core region of the parsec-scale jet. They proposed a spine-sheath model to interpret the synchronous optical and radio polarization variability, including all the characteristics of the observed emission: the time-variable flux density S(ν,t), polarization degree p(ν,t) and polarization angle PA(ν,t).

characteristics of the optical multi-wavelength flux density and polarization for OJ287.

The results restated above for the quasi-periodic optical outbursts in 1971.7, 1973.0, 1983.0 and 2005.7 show that they are all nonthermal flares, produced within the relativistic jet, and support the lighthouse model (or helical motion model) proposed in Qian (2019).

It can be seen from the above description that multi-frequency observations in optical/IR and radio/millimeter wavebands (measuring time-variable flux density curve, polarization degree curve and polarization angle curve) are very important to understand the nature of optical emission in OJ287. Search for correlation between the optical and radio outbursts can provide decisive evidence for the mechanism producing the optical radiation. In this paper we will investigate the optical-radio correlation for the quasi-periodic optical outburst event in 1995.8.

We would like to point out that a variety of connections between optical and radio variability has been observed in OJ287, involving different emitting processes: e.g., (1) simultaneous radio-optical bursts; (2) radio bursts delayed with respect to optical bursts (e.g., Valtaoja et al. 1987, 2000); (3) radio bursts without optical counterparts; (4) optical bursts without radio counterparts, etc. Superluminal optical knots, which produce simultaneous radio-optical emission through lighthouse effect near the nucleus, may continue to move outward and evolve to form superluminal radio knots on parsec scales, causing delayed connection between radio and optical outbursts (e.g., Britzen et al. 2018, Qian 2018, Agudo et al. 2012, Sillanpää et al. 1985, Valtaoja et al. 2000, Tateyama et al. 1999, Kushwaha et al. 2018a, Aller et al. 2014).

3. Assumptions

In the following, we will continue to explore the optical and radio variability behavior in OJ287 in terms of the lighthouse model under the precessing jet nozzle scenario and concentrate on investigating the connection between the radio/millimeter and optical flares observed during the quasi-periodic outburst event in 1995.84, and further show that the simultaneous variability behavior at radio/millimeter and optical wavelengths support the lighthouse model proposed in Qian (2019).

3.1. Geometric parameters

We will use the same formulation and parameters to describe the precessing jet-nozzle scenario and the helical model, referring to Qian (2019) for details. The geometric parameters for the model simulation are listed in Table 1. We assume that superluminal knots move along helical trajectories (probably helical magnetic fields) around the jet axis, which is shown in Figure 1 (left panel). The jet axis precesses around the precession axis (not displayed here) which is defined by parameters ϵ and ψ. The selected jet axis is defined by precession phase ω=–2.0 rad. The jet

axis is described by parameters a and x, which define a straight line. The helical trajectory pattern is defined by the parameters A (amplitude) and $\mathrm{d}\phi/\mathrm{d}z_0$ (rotation rate). In the right panel of Figure 1 the modeled Lorentz factor and Doppler factor are shown for the elementary flare in 1995.98 (peaking at JD2450075).

3.2. Spectra of elementary flares

As suggested in Qian (2019) that the quasi-periodic outbursts can be decomposed into several elementary flares with symmetric profiles and each elementary flare can be explained in terms of the lighthouse model. Thus the light-curves observed in optical and radio/mm wavebands can be simulated. We assume that the elementary flares have broken power-law spectra in the NIR–optical–UV bands with a spectral break at V-band of $\Delta\alpha$= 0.5 and the local V-band spectral index $\alpha_{\rm v}$=1.0 ($S_\nu \propto \nu^{-\alpha}$). The flux densities of the underlying jet (or base-levels) are assumed to be constant and listed in Table 2. The modeled radio/mm spectra are described in terms of the modeled indexes between the radio/mm and V-band. As an example, in Figure 2 is shown the modeled radio-optical spectrum for the elementary flare in 1995.98 (peaking at JD2450075). The modeled flux densities are listed in Table 3. The corresponding comoving (or intrinsic) flux densities are listed in Table 4.
It should be noted that the local spectral index in the radio-mm region (8 GHz to 37 GHz) is much smaller than that at V-band ($\alpha_{\rm v}$=1.0; see Figure 2), and thus the variability amplitudes of the radio/mm outbursts will be much smaller than that in the optical V-band (see below).

3.3. Doppler boosting and simulation of optical light-curve

We will model simulate the V-band optical light-curve of the 1995.84 outburst event in terms of the lighthouse model proposed in Qian (2019). In this case the lighthouse effect results in a symmetric light-curve via Doppler boosting per revolution of the helical motion for each of elementary flares. The observed optical flux density can be written as:

$$S_{\rm v,obs}(t) = S_{\rm v,co}\times[\delta(t)]^{3+\alpha_{\rm v}} + S_{\rm b,v} \quad (1)$$

Where $S_{\rm v,co}$(t) represents the constant comoving (or deboosted) optical flux density, δ(t)–Doppler factor of the superluminal optical knot, $\alpha_{\rm v}$–local spectral index at V-band (Blandford & Königl 1979), assumed to be $\alpha_{\rm v}$=1.0. $S_{\rm v,b}$– the underlying flux density of the jet at V-band (Table 2). The modeled Lorentz factor Γ, Doppler factor δ and comoving flux density $S_{\rm v,co}$ are selected for each of the elementary flares to reasonably fit the entire optical light-curve (see Table 5).

3.4. Parameters for simulation of radio/mm light-curves

For model simulation of the radio/millimeter light-curves at frequencies of 8, 14.5, 22, and 37 GHz, we will define the modeled two-point spectral indexes α(radio,v) between the radio/mm frequencies and V-band frequency: α(37GHz,v), α(22GHz,v), α(15GHz,v) and α(8GHz,v). The modeled radio/mm light-curves will be derived from the modeled V-band light-curve using the formula given in equation (2).

$$S_{\rm radio} = S_{\rm v}\times[\nu_{\rm radio}/\nu_{\rm v}]^{-\alpha({\rm radio,v})} \quad (2)$$

$S_{\rm radio}$ represents the modeled flux density at the radio frequencies of 8, 14.5, 22 and 37 GHz. $S_{\rm v}$ represents the modeled V-band optical flux density. The modeled spectral indexes α(radio,v) are selected to reasonably fit the observed radio/mm light-curves (see Tables 5 and 6). This method is equivalent to select appropriate two-point radio spectral indexes α(22GHz,37GHz), α(14.5GHz,37GHz) and α(8GHz,37GHz) to simulate the radio light-curves at 22, 14.5 and 8 GHz, when the 37 GHz light-curve is fitted by using α(37GHz,V-band).

3.5. Cosmological model

In this work, we adopt a ΛCDM cosmological model with the parameters as: $\Omega_m = 0.27$, $\Omega_\Lambda = 0.73$ and $\mathrm{H_0}$=71 km s^{-1} Mpc^{-1} (Spergel et al. 2003, Komatsu et al. 2009). 1 mas = 4.5 pc (Hogg, 1999).

4. Connection between optical and radio/millimeter outbursts

The light curves observed during the period 1995.77 (JD2450000) – 1996.13 (JD2450130) in the optical V-band and radio/mm bands (37, 22, 14.5 and 8 GHz) are shown in Figure 3. The V-band data were taken from Basta & Hudec (2006) and OJ-94 project (Nilsson, private communication). The 37 and 22 GHz data were taken from Valtaoja et al. (2000) and the 14.5 and 8 GHz data from UMRO-archive (Aller, private communication).
It can be seen that the optical light curve consists of a large number of elementary spike-like flares with time scales of days. Figure 3 shows that the envelopes of the radio/mm light curves are much more smoother than that of the optical light-curve. This is due to the local spectral indexes at radio/mm wavelengths are much smaller than that at optical V-band ($\alpha_{\rm v}$=1.0). However, even by visual inspection it can be seen that the radio/mm light-curves have their envelopes very similar to that of the optical envelope during the period JD2450060–2450090. Very clearly, for the 37 and 22 GHz light curves this similarity in the envelopes can be extended to JD2450120 when both the optical flux density and the 37–22 GHz flux densities simultaneously reached to their quiet levels. Moreover, a few optical spikes (e.g, at JD2450075 and JD2450080) can be recognized to have their concurrent flares in the 37 and 22 GHz light-curves. All these similarities in the radio/mm and the optical variations clearly demonstrate that the radio/mm flares are simultaneous with the optical flares without measurable time delays (less than two days), as suggested previously by Valtaoja et al. (2000).
The close connection between the radio/mm outbursts at four frequencies (37, 22, 14.5 and 8 GHz) and the optical outburst (or simultaneous variability behavior) during the period of 1995.8–1996.1 provides further evidence for the nonthermal nature of the quasi-periodic optical outbursts in OJ287, in addition to the association of the high energy γ-ray and optical outbursts. [6] The close connection between the optical and radio/mm outbursts may be regarded as another decisive evidence that the optical outbursts and their constitutive (elementary) flares in OJ287 are synchrotron

[6] Also see the results of the correlated optical and multi-waveband radio/mm outbursts observed in 1971–1974 (Usher 1979).

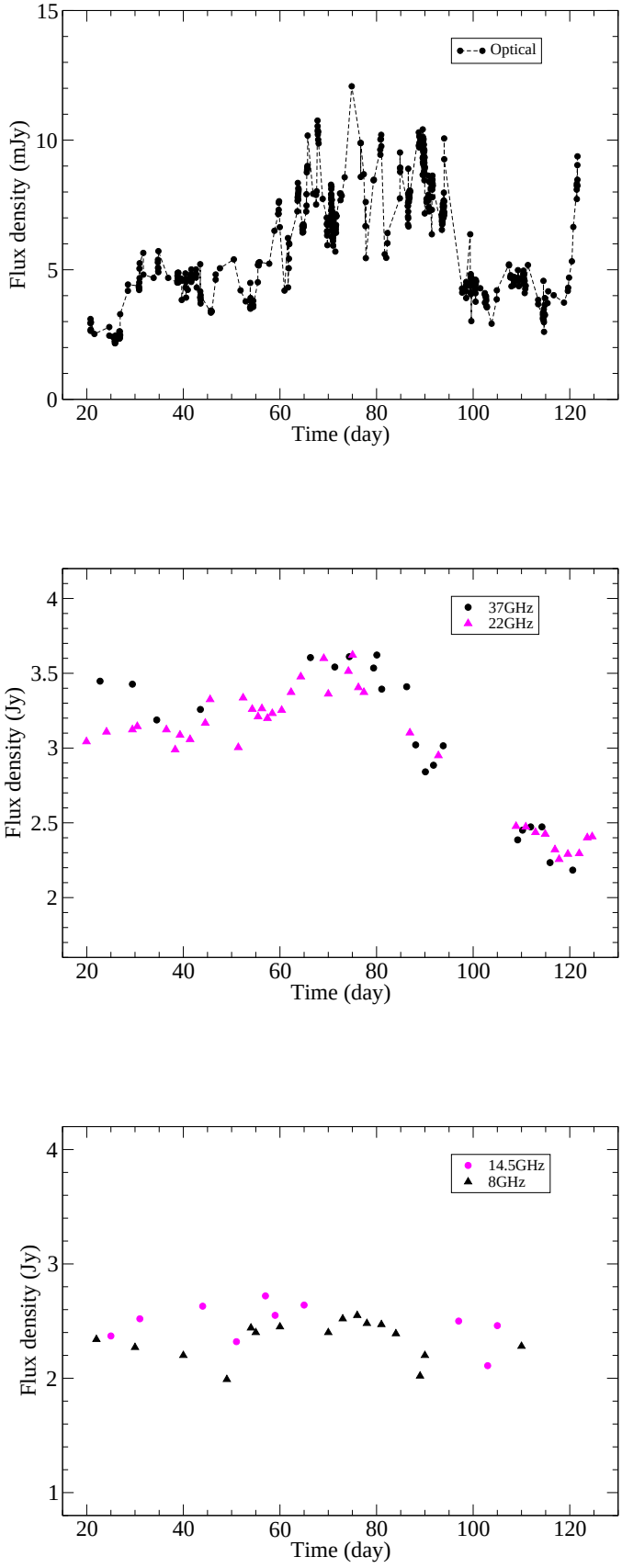


Fig. 3. Quasi-periodic optical outburst in 1995.84: optical V-band light curve (upper panel) and radio/millimeter light curves observed at 37/22 GHz (middle panel) and 14.5/8 GHz (bottom panel). Zero point of time=Julian date 2450000 (1995.7735).

in origin. The arguments against lighthouse models (e.g., Valtaoja et al. 2000) can now be clarified.
(1) Firstly, in the precessing jet nozzle scenario, both the optical and radio/mm outbursts are due to enhanced Doppler boosting induced by lighthouse effect due to the helical motion of the same superluminal knots. Thus the radio emissions are similarly boosted. Due to the nature of synchrotron emission the polarization properties in optical and radio/mm wavebands can be well interpreted.
(2) The interpretation of both the optical and radio/mm outbursts in terms of the precessing jet nozzle models does not involve precession of the whole jet. Thus the emissions in optical and radio/mm wavebands from the underlying jet (or the quiescent base-levels) do not experience Doppler boosting during the outbursts.
(3) The lighthouse model proposed here requires the emitting source having some kind of radiation structure (or distribution): the radio/mm and optical emission do not come from the exactly same region. Most possibly, it could be a planar shock front with a core-envelope structure. Its central (core) region dominates the emission in IR-optical bands (and the associated γ-rays), while its outer region (envelope) dominates the emission in radio/mm wavebands. Thus the optical and radio/mm emissions can be simultaneously and similarly Doppler boosted, when the source moves along helical trajectories, if the shock front is perpendicular to the direction of the motion. This core-envelope structure is consistent with the concept of the stratification of magnetic surface structure in the magnetospheres of spinning black hole-accretion disk systems (e.g., Camenzind,1990).
(4) The radio/mm emitting regions may have different optical depths or opacity effects in different cases. This can explain why some quasi-periodic optical outbursts do not have radio counterparts. But even in these cases delayed radio outbursts are usually observed if the optical knots evolve to form pure radio knots in outer jet regions on parsec scales (Valtaoja et al. 2000, Tateyama et al. 1999, Britzen et al. 2018, Qian 2018).
(5) Our studies (Qian 2019 and this work) have found that the quasi-periodic optical outbursts can be decomposed into several elementary flares, each having symmetric profiles with similar rising and declining timescales. This explains why the individual flares during quiescent period and flaring period have similar variability timescales (Valtaoja et al. 2000), because the elementary flares during quiescent and flaring periods have similar properties: flux density is boosted and timescale is compressed by Doppler effects.
(6) Since the flux enhancements induced by Doppler boosting depend on the local spectral index at the emission frequency, the flattening of the radio/mm spectrum with respect to the IR-optical spectrum results in the amplitude of the radio/mm outbursts being much smaller than that of the optical outbursts, as usually observed.
(7) This work only investigate the interpretation of the optical and radio/mm outbursts (related to superluminal knots) on timescales of ∼10–100 days. Thus the underlying jet flux density (or the base-level flux density) is assumed to be constant. However, the physical conditions of the jet (jet bulk motion and magnetic field structure, etc.) should vary on longer time-scales and the jet precession (with a period of ∼12 yr) will also modulate the underlying jet emission. In order to understand the whole phenomena in OJ287 all these ingredients should be taken into consideration.

In the following we will model simulate the optical and radio/mm light curves in terms of lighthouse effect due to the helical motion of the superluminal optical/radio knots, respectively.

4.1. Model simulation of the optical light-curve

Since the quasi-periodic optical outbursts can be decomposed into several elementary outbursts and each of the elementary flares can be interpreted in terms of the helical motion model, we can use the processing jet nozzle model and the kinematic properties observed on parsec scales to investigate the light-curves of optical outbursts in OJ287.
The model simulation of the optical light-curve for the 1995.84 outburst event is shown in Figure 4. The model parameters and results for all the optical elementary flares are summarized in Table 5: $t_{\rm peak}$ (JD–2450000) – peaking epoch of elementary flare; $S_{\rm v}$ (mJy) – optical flux density at peak; $S_{\rm b}$ (mJy) – base-level (underlying jet) flux density; Γ – bulk Lorentz factor of superluminal optical knots; $\delta_{\rm max}$ – maximum Doppler factor; r – ratio of the maximum and minimum Doppler factor; $S_{\rm v,co}$ (mJy) – comoving (or deboosted) flux density and the numbers in the parentheses represent the powers of 10; FWHM (day) – full width at half-maximum of flare profile.
Due to the insufficient sampling of the optical observations it is very difficult to recognize the discrete elementary flares. The simulation is certainly not unique, depending on personal assessments on the decomposition. We have tried to recognize the symmetric distributions of the data-points. The simulation results described here may provide us useful information about the elementary flares: timescale, bulk motion Lorentz factor, Doppler beaming factor, comoving optical flux density etc., which may be useful to understand the nature of the optical outbursts, jet physics, superluminal knot kinematics and the characteristics of the putative central black hole binary system.
For describing the simulation results we divide the light-curve into three segments: segment I for time-interval JD2450024–2450049 (1995.8392–1995.9077; 25 days), segment II for time-interval JD2450050–2450097 (1995.9104–1996.0391; 47 days) and segment III for time-interval JD2450098–2450118 (1996.0418–1996.0966; 20 days).

4.1.1. Segment I

This part of the light-curve may be regarded as the starting stage of the 1995.84 outburst event. Epoch JD2450024 (1995.841) has been predicted as the starting epoch of the primary thermal outburst in the disk-impact model, but this impact-outburst did not happen and the source retained at a low activity level within the first 25 days: neither a strong burst nor a standard impact-burst light curve was observed, while the follow-up synchrotron flares happened as usual. The disappearance of the primary impact-outburst seems difficult to be understood under the disk-impact scenario, and the claimed timing of this impact-outburst seems losing its physical meaning.
Applying the lighthouse model we use ten elementary flares with similar symmetric profiles to fit the light-curve, which is displayed in upper panel of Figure 4. Although the data sampling is very sparse, the elementary flares (at $t_{\rm peak}$=27.86, 31.36, 34.46, 39.26, 41.06, 42.86 and 46.41) can

Table 5. Model-simulation parameters for the 36 elementary flares at V-band. $t_{\rm peak}$ (JD–2450000) – peaking epoch of the modeled elementary flares: 1995.840 is corresponding to Julian date (JD) 2450024.29. Base-level flux density $S_{\rm v,b}$=2.70 mJy. $S_{\rm v,p}$ (mJy) – modeled peak flux density. Γ – bulk Lorentz factor of the optical knot. $\delta_{\rm max}$ – maximum Doppler factor, r=$\delta_{\rm max}/\delta_{\rm min}$, $S_{\rm v,co}$ (mJy) – modeled comoving (or deboosted) flux density. FWHM (day) – full width at half-maximum of the elementary flare profile.

$t_{\rm peak}$	$S_{\rm v,p}$(mJy)	Γ	$\delta_{\rm max}$	r	$S_{\rm v,co}$(mJy)	FWHM
27.86	6.54	17.0	33.58	10.95	3.03(-6)	1.0
31.36	6.54	17.0	33.54	10.94	3.03(-6)	1.0
34.46	6.54	17.0	33.54	10.94	3.03(-6)	1.0
37.66	6.54	17.0	33.54	10.94	3.03(-6)	1.0
39.26	6.54	17.0	33.54	10.94	3.03(-6)	1.0
41.06	6.54	17.0	33.54	10.94	3.03(-6)	1.0
42.86	6.54	17.0	33.54	10.94	3.03(-6)	1.0
44.56	6.54	17.0	33.54	10.94	3.03(-6)	1.0
46.41	6.54	17.0	33.54	10.94	3.03(-6)	1.0
47.76	6.54	17.0	33.54	10.94	3.03(-6)	1.0
50.81	6.54	17.0	33.54	10.94	3.03(-6)	1.0
52.21	6.54	17.0	33.54	10.94	3.03(-6)	1.0
54.76	6.54	17.0	33.54	10.94	3.03(-6)	1.0
56.35	6.43	14.0	27.73	7.76	6.32(-6)	1.8
59.29	7.47	12.5	24.79	6.39	1.26(-5)	2.5
63.07	7.83	13.0	25.77	6.83	1.16(-5)	2.3
65.95	9.04	14.0	27.73	7.76	1.07(-5)	1.8
68.12	12.0	14.5	28.70	8.25	1.37(-5)	1.5
70.30	10.9	17.5	34.51	11.5	5.81(-6)	0.9
71.95	10.4	16.5	32.58	10.4	6.82(-6)	1.0
75.05	12.3	11.5	22.82	5.56	3.53(-5)	3.3
77.06	6.61	15.0	29.67	8.75	5.05(-6)	1.3
80.32	11.7	14.5	28.70	8.25	1.32(-5)	1.6
85.16	8.79	12.0	23.81	5.97	1.89(-5)	3.0
88.96	10.1	12.0	23.81	5.97	2.32(-5)	3.0
92.12	9.22	14.5	28.70	8.25	6.66(-6)	1.6
94.98	10.4	13.5	26.75	7.29	1.50(-5)	2.2
99.06	6.54	17.0	33.54	10.94	3.03(-6)	1.0
101.02	6.54	17.0	33.54	10.94	3.03(-6)	1.0
103.17	6.54	17.0	33.54	10.94	3.03(-6)	1.0
105.62	6.54	17.0	33.54	10.94	3.03(-6)	1.0
107.11	6.54	17.0	33.54	10.94	3.03(-6)	1.0
108.90	6.54	17.0	33.54	10.94	3.03(-6)	1.0
111.15	6.54	17.0	33.54	10.94	3.03(-6)	1.0
113.83	6.54	17.0	33.54	10.94	3.03(-6)	1.0
116.17	6.54	17.0	33.54	10.94	3.03(-6)	1.0
122.10	10.4	13.5	26.75	7.29	1.50(-5)	2.2

reasonably well fit the data-points, implying steady ejections of superluminal optical knots with similar properties during this time-interval. All the optical knots are modeled with the same bulk Lorentz factor of Γ=17, having time-scales of $\sim$1 day.

4.1.2. Segment II

This segment of the light-curve may be regarded as the main part of the optical event starting in 1995.84, revealing a group of large amplitude spike-like flares and an envelope of typical pattern of rising-plateau-declining stages. Although the data sampling is still insufficient to accurately decide the peak epoch and amplitude of these spikes, the decomposition of the outburst into its elementary flares can be made appropriately. Seventeen elementary flares with different Lorentz factors (in the range of 11.5 to 17.5) have been used (see Table 5). The simulation results are displayed in the middle panel of Figure 4. The bold violet curve denotes the modeled total flux density, which reasonably well fit most of the observational data-points. The elementary flares have their time-scales in the range of 0.9 to 3.3 days.

4.1.3. Segment III

This segment may be regarded as the ending stage of the outburst event, when the flaring activity sharply declined. Nine elementary flares with similar symmetric profiles and Lorentz factors (Γ=17) has been used to simulate the light-curve. Although the data sampling is insufficient to accurately decide their peak amplitudes, the elementary flares (at $t_{\rm peak}$=99.06, 101.02, 108.90, 111.15, 113.83 and 116.17) can reasonably well fit the observational data-points. After JD2450120 another activity period started.

As a brief summary, it can be seen that the entire light-curve of the optical outburst event staring in 1995.84 (JD2450024) during a period of $\sim$3 months can be model-simulated in terms of our lighthouse model (helical motion model). All these elementary flares have symmetric profiles

with similar Lorentz factors and time-scales. Their comoving (or de-boosted) flux densities are on order of 10^{-6} mJy, implying that the Doppler boosting effects are very strong. The characteristics of the superluminal optical/radio knots and their helical motion explored in this work may be significant for understanding the nature of the whole phenomena in OJ287.

4.2. Model simulation of 37 GHz light curve

Corresponding to the simulation of the optical light-curve, the 37 GHz light-curve has been simulated and shown in Figure 5. The modeled 37 GHz light curve is derived from the modeled optical light-curve by selecting the spectral index α(37GHz,V-band) between 37 GHz and optical V-band for each of the elementary flares which are listed in Table 6. The 22 GHz light-curve can be fitted using a similar method by selecting spectral index α(22GHz,V-band) for the elementary flares, but the fitting results are not given here. However, the 22 GHz data-points are also shown in Figure 5 to help visual-inspecting the quality of the simulation of the 37 GHz light-curve. The simulation results are described separately for three segments as follows.

4.2.1. Segment I

Corresponding to the same segment of the optical light-curve (JD2450024–2450049), ten elementary flares at 37 GHz are simulated (upper panel of Figure 5). Unfortunately, only three data-points are available, but the data-point at $t_{\rm peak}$=34.46 is well fitted, coincided with the optical flare. There are four 22 GHz data-points very close to the profile of the flares at $t_{\rm peak}$=37.66, 39.26, 41.06 and 44.56, indicating that the optical flares should have their counterparts at 37 GHz. The 37 and 22 GHz data-points between 2450028 and 2450030 have no optical counterpart, possibly implying the existence of a pure radio/mm burst.

4.2.2. Segment II

Corresponding to the main part of the optical light-curve seventeen 37 GHz elementary flares are simulated and the results are shown in the middle panel of Figure 5. The bold violet curve denotes the modeled total flux density curve. It can be seen that almost all the 37 GHz data-points are reasonably well fitted (within uncertainty of ∼1-2 days), indicating their simultaneous flaring at optical and 37 GHz wavelengths. In particular, the optical peak at $t_{\rm peak}$=80.32 has a well fitted 37 GHz peak. During the time-interval between 2450050 and 2450078, the 22 GHz data-points are close to the profiles of the 37 GHz elementary flares, demonstrating the simultaneous variations at 37/22 GHz and optical wavelengths.

4.2.3. Segment III

Corresponding to the same part of the optical light-curve, nine 37 GHz elementary flares have been used in the simulation. The results are displayed in the bottom panel of Figure 5. Only five data-points are available and four elementary flares are invoked, having very low flux densities and a spectral index α(37GHz,V-band) of 0.40, much smaller than those (0.50–0.58) during the outburst peaking stage (between 2450050 to 2450085; see Table 6). It can be seen from Figure 5 (middle panel) that the observed 22 GHz light-curve is slightly below the 37 GHz light-curve, thus introduction of spectral index α(22GHz,V-band) slightly smaller than the α(37GHz,V-band), will well fit the 22 GHz light curve.

As shown above, we can reasonably well explain the optical and 37–22 GHz light curves in terms of the lighthouse model under the precessing jet nozzle scenario. Each of the optical elementary flares have their 37/22 GHz counterparts. Same Doppler boosting factors are effective for both optical and radio/mm flares. These results can not be obtained in the whole-jet precessing models (e.g., Valtaoja et al. 2000).

The significant point is that the 37–22 GHz elementary flares are shown to be synchronous with the optical ones. If the 37–22 GHz flares were delayed with respect to the optical flares, the spikes on time-scales of ∼1-2 days in the 37–22 GHz light-curves might have been smoothed out and have not been observed.

4.3. Model simulation of 14.5 GHz light curve

The model-simulation results for the 14.5 GHz light-curve are displayed in Figure 6. As for the 37 GHz light-curve, the modeled 14.5 GHz light-curve is derived from the optical light-curve by selecting the spectral index α(15GHz,V-band) for each of the thirty-six 14.5 GHz elementary flares, which are listed in Table 7. The simulation results are separately described for three segements.

4.3.1. Segment I

Only three 14.5 GHz data-points are available in this time-interval (JD2450024–2450049), we cannot make any meaningful conclusion about the model-fitting. However, two data-points are close to the peaks of the elementary flares at $t_{\rm peak}$=31.36 and 44.56 within uncertainty of ∼1 day, showing the modeled light-curve close to the observed level of 14.5 GHz flux density. In this time-interval the spectral index $\alpha_{15,\rm v}$ was assumed to be 0.54.

4.3.2. Segment II

For the main part of the optical outburst, the 14.5 GHz light-curve has been simulated in terms of the lighthouse model. The four 14.5 GHz data-points are reasonably well fitted (within uncertainty of ∼1-2 days) by the modeled total flux density curve at $t_{\rm peak}$=50.8, 56.35, 59.29 and 65.95. In addition, ten 8 GHz data-points in the time-interval between 2450050 and 2450089 are close to the modeled 14.5 GHz total flux density curve, indicating the simultaneous variations at 14.5–8 GHz and optical wavelengths.

4.3.3. Segment III

Although only three data-points are available in this time-interval (JD2450090–2450118), two data-points are reasonably well fitted by the modeled total flux curve at $t_{\rm peak}$=103.17 and 105.62 within uncertainty of ∼1 day. The 14.5 GHz data-point near JD2450097 might indicate the existence of a radio burst not associated with any optical

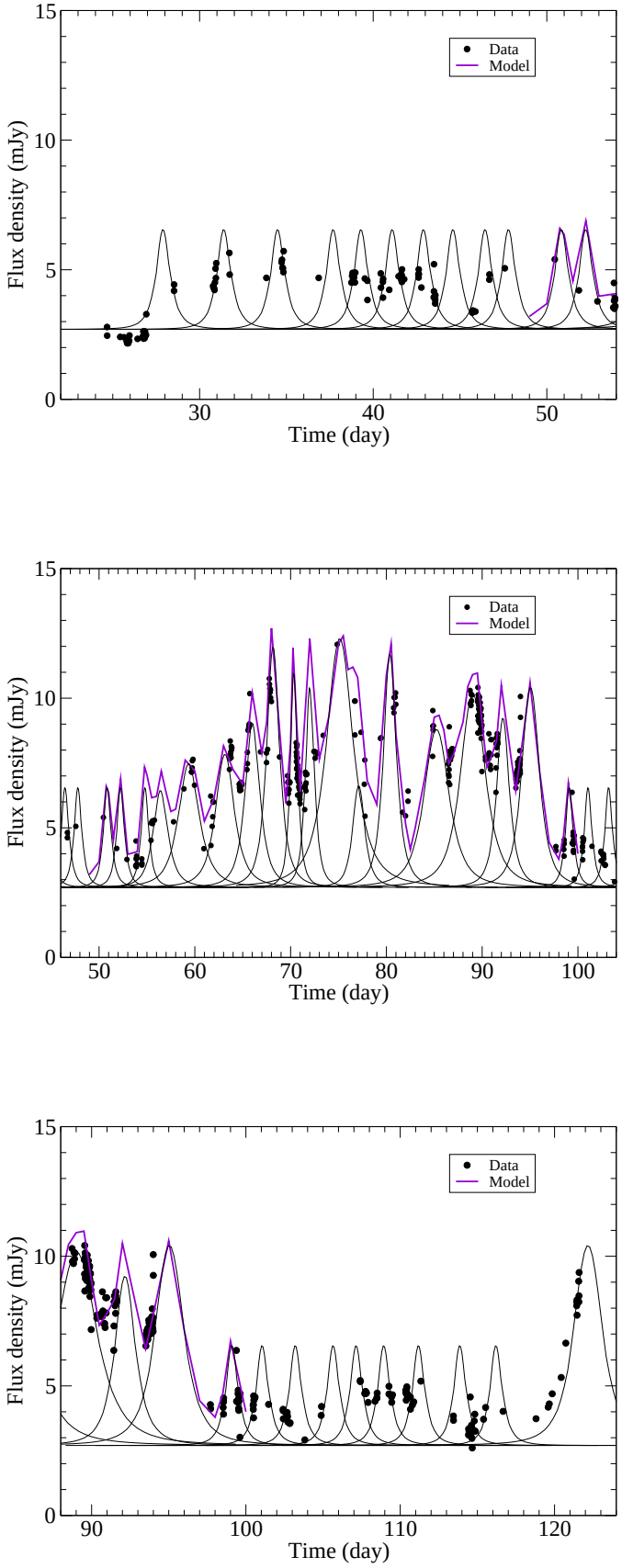


Fig. 4. Model simulation of the optical light curve for the 1995.8 optical outburst event (1995.84–1996.10): the light curve is displayed in three segments, separately. The model parameters are listed in Table 5.

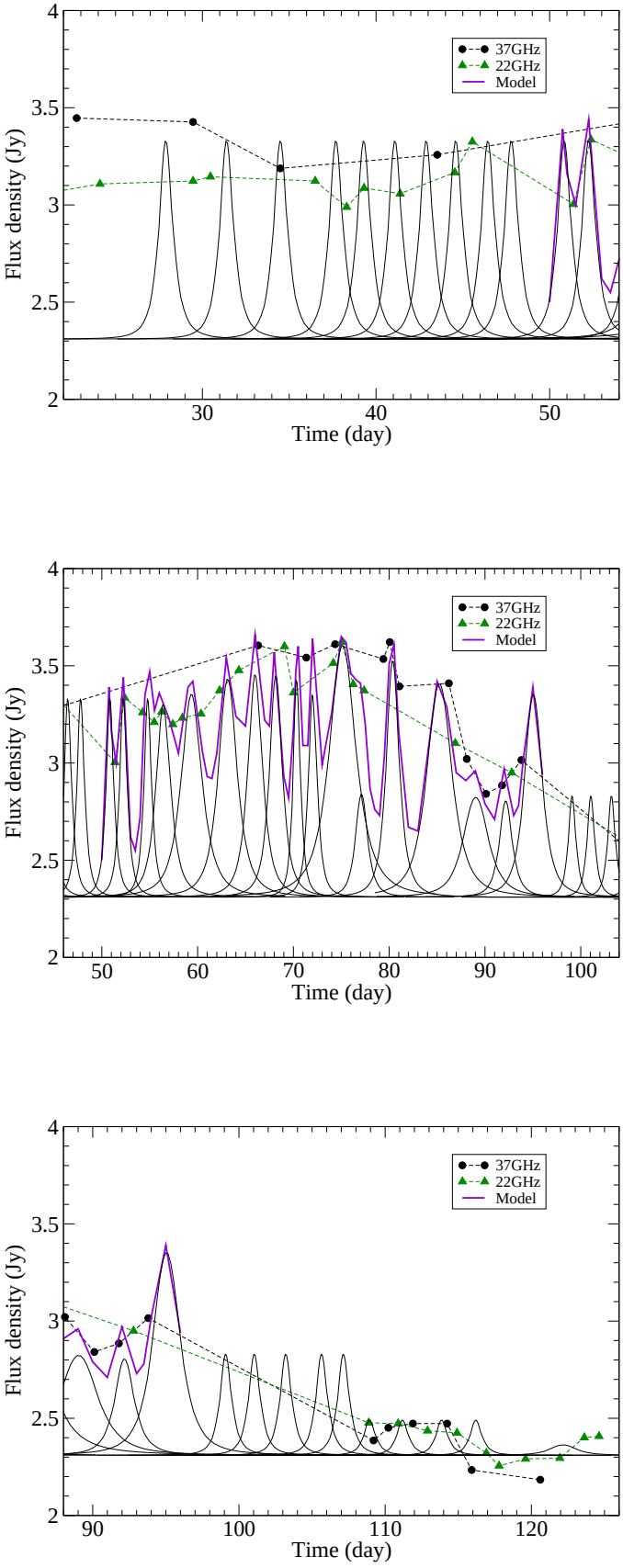


Fig. 5. Model simulation of the 37 GHz light curve during the outburst event between 1995.84 and 1996.10 (JD2450024–2540118). The model parameters are listed in Table 6.

Table 6. Model-simulation parameters for the thirty-six elementary flares at 37 GHz. $S_{\rm b,37}$=2.31 Jy.

$t_{\rm peak}$	$S_{37,\rm p}$	$\alpha_{37,\rm v}$	$S_{37,\rm co}$
27.86	3.33	0.58	8.00(-7)
31.36	3.33	0.58	8.00(-7)
34.46	3.33	0.58	8.00(-7)
37.66	3.33	0.58	8.00(-7)
39.26	3.33	0.58	8.00(-7)
41.06	3.33	0.58	8.00(-7)
42.86	3.33	0.58	8.00(-7)
44.56	3.33	0.58	8.00(-7)
46.41	3.33	0.58	8.00(-7)
47.76	3.33	0.58	8.00(-7)
50.81	3.33	0.58	8.00(-7)
52.21	3.33	0.58	8.00(-7)
54.76	3.33	0.58	8.00(-7)
56.35	3.30	0.58	1.67(-6)
59.29	3.35	0.56	2.76(-6)
63.07	3.43	0.56	2.54(-6)
65.95	3.45	0.54	1.93(-6)
68.12	3.45	0.50	1.69(-6)
70.30	3.42	0.51	7.85(-7)
71.95	3.35	0.51	9.22(-7)
75.05	3.61	0.51	4.77(-6)
77.06	2.84	0.51	6.81(-7)
80.32	3.52	0.51	1.79(-6)
85.16	3.41	0.54	3.42(-6)
88.96	2.82	0.44	1.59(-6)
92.12	2.80	0.45	7.22(-7)
94.98	3.35	0.51	2.03(-6)
99.06	2.83	0.51	4.11(-7)
101.02	2.83	0.51	4.11(-7)
103.17	2.83	0.51	4.11(-7)
105.62	2.83	0.51	4.11(-7)
107.11	2.83	0.51	4.11(-7)
108.90	2.49	0.40	1.42(-7)
111.15	2.49	0.40	1.42(-7)
113.83	2.49	0.40	1.42(-7)
116.17	2.49	0.40	1.42(-7)
122.10	2.36	0.20	0.98(-7)

flare.

4.4. A brief summary

We have investigated the correlation between the optical flares and radio/mm bursts on timescales of days in OJ287 for the 1995.84 optical outburst event. The aim is to search the clues for the lighthouse effect which produces the simultaneous optical and radio/mm elementary flares with symmetric profiles. Obviously, the observation data currently available at 37, 22, 14.5 and 8 GHz are too sparse to fulfill this task. However, we find that at least for the main part of the optical outburst between JD2450050 and 2450090, the modeled total flux curves at 37 GHz and 14.5 GHz wavelengths reveal variations on short time-scales which can reasonably well fit the observed radio peaks associated with the optical peaks. Thus the lighthouse effect in producing the optical and radio/mm flares during the 1995.8 outburst event has been confirmed. In order to further explore the correlation between the optical and radio/mm variations on short time-scales in OJ287, more contemporary observations at optical and radio/mm wavelengths on daily sampling rates are required.

We further point out that the superluminal optical knots producing the simultaneous optical and radio/mm flares near the nucleus should continue to move outward along their trajectories and evolve to form superluminal radio knots on parsec scales, which emit at radio wavelengths, appearing as delayed radio flares.

5. Discussion

We have applied the precessing jet nozzle scenario previously proposed by Qian et al. (e.g., 1991, 2013, 2019) to investigate and simulate the correlation between the variations at optical and radio wavelengths for the quasi-periodic optical outburst event during 1995.84–1996.10. Since the radio/mm data are very sparsely sampled, this work can only be regarded as a preliminary examination. However, we have found convincing evidence that the optical outburst can be decomposed into a group of elementary flares and each of the optical elementary flares emits simultaneous radio/mm emission. The simultaneous optical and radio/mm variations can be reasonably well interpreted in terms of lighthouse effect due to the helical motion of the discrete superluminal optical/radio knots.

Combining with the results obtained in Usher (1979),

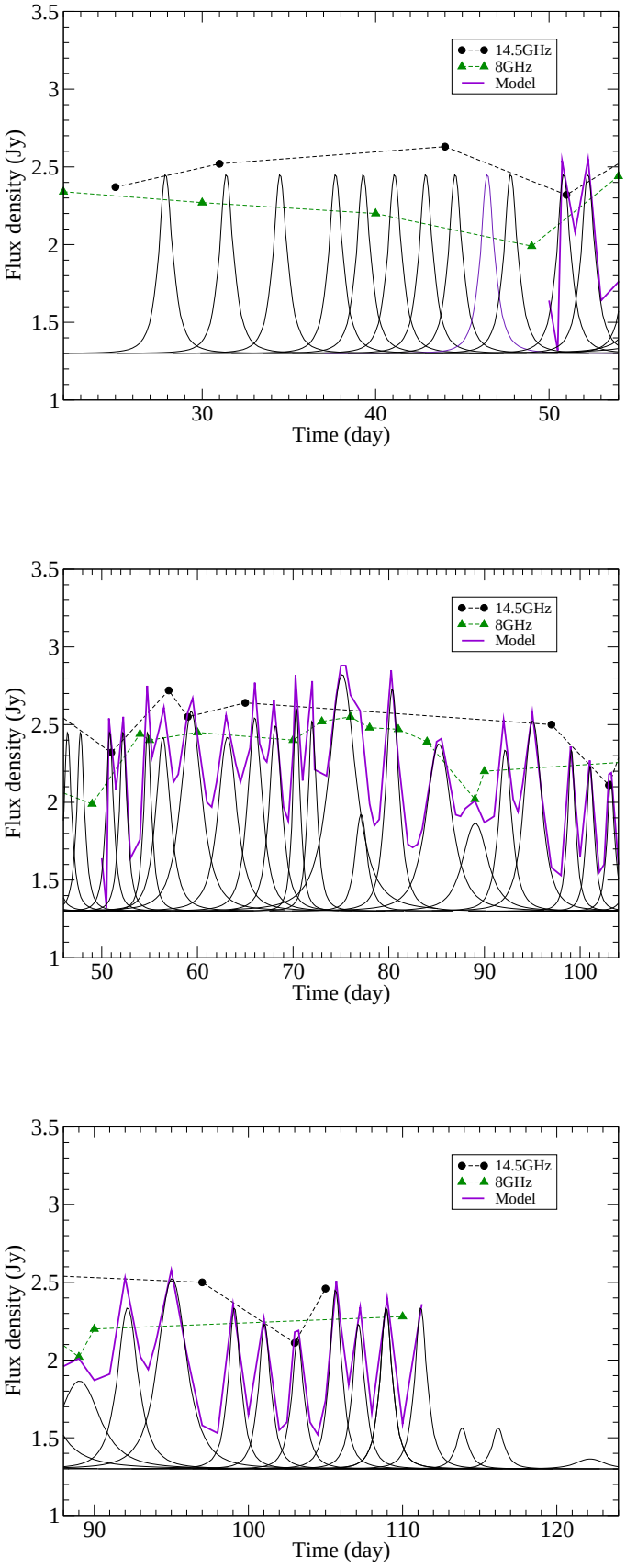


Fig. 6. Model simulation of the 14.5 GHz light curve. The model parameters are listed in Table 7.

Table 7. Model-simulation parameters for the thirty-six elementary flares at 14.5 GHz. S_b=1.30 Jy.

$t_{\rm peak}$	$S_{15,\rm p}$	$\alpha_{15,\rm v}$	$S_{\rm co,15}$
27.86	2.45	0.54	9.03(-7)
31.36	2.45	0.54	9.03(-7)
34.46	2.45	0.54	9.03(-7)
37.66	2.45	0.54	9.03(-7)
39.26	2.45	0.54	9.03(-7)
41.06	2.45	0.54	9.03(-7)
42.86	2.45	0.54	9.03(-7)
44.56	2.45	0.54	9.03(-7)
46.41	2.45	0.54	9.03(-7)
47.76	2.45	0.54	9.03(-7)
50.81	2.45	0.54	9.03(-7)
52.21	2.45	0.54	9.03(-7)
54.76	2.45	0.54	9.03(-7)
56.35	2.42	0.54	1.89(-6)
59.29	2.58	0.53	3.40(-6)
63.07	2.42	0.51	2.54(-6)
65.95	2.54	0.50	2.10(-6)
68.12	2.49	0.46	1.75(-6)
70.30	2.61	0.48	9.92(-7)
71.95	2.52	0.48	1.08(-6)
75.05	2.82	0.48	5.60(-6)
77.06	1.92	0.48	8.01(-7)
80.32	2.73	0.48	2.10(-6)
85.15	2.37	0.49	3.33(-6)
88.96	1.86	0.41	1.74(-6)
92.12	2.33	0.48	1.52(-6)
94.98	2.52	0.48	2.39(-6)
99.06	2.33	0.53	8.14(-7)
101.02	2.23	0.52	7.35(-7)
103.17	2.14	0.51	6.64(-7)
105.62	2.45	0.54	9.09(-7)
107.11	2.23	0.52	7.35(-7)
108.90	2.33	0.53	8.14(-7)
111.15	2.33	0.53	8.14(-7)
113.83	1.56	0.40	2.06(-7)
116.17	1.56	0.40	2.06(-7)
122.10	1.36	0.20	1.17(-7)

Holmes et al. (1984), D'Arcangelo et al. (2009) and Qian (2019), we may tentatively suggest that the quasi-periodic double-peaked outbursts in 1971–1973, 1983–1984, 1994–1995, 2005–2006 and the outburst in 2015.76 are synchrotron flares produced within its relativistic jets in OJ287. The superluminal optical/radio knots may have some kind of stratified core-envelope structure [7] with its core region dominating the optical emission and the outer regions dominating the mm/radio emission. Thus the optical and radio emission from the superluminal knots can be Doppler boosted simultaneously due to lighthouse effect during their helical motion.

Helical motion of superluminal knots may be expected on the basis of magnetodynamic (MHD) theories for jet formation in spinning black-hole and accretion-disk systems, in which relativistic jets are produced in the rotating magnetospheres with strong toroidal magnetic fields. Thus helical fields should permeate in the inner jet regions near the black holes (e.g., Blandford & Znajek 1977, Blandford & Payne 1982, Camenzind 1990, Li et al. 1992, Beskin 2010, Vlahakis & Königl 2004, Meier 2013, 2001). It would be a natural phenomenon that superluminal optical knots move along helical trajectories, producing optical outbursts through lighthouse effect. Unfortunately, only a few optical events have been observed revealing this phenomenon (e.g., Schramm et al. 1993, Dreissigacker 1996a, Dreissigacker & Camenzind 1996b, Camenzind & Kronkberger 1992, Wagner et al. 1995).

This work further strengthens the arguments proposed in Qian (2019 that helical motion of superluminal optical knots may prevail in blazar OJ287 and produce both quasi-periodic and non-periodic optical outbursts, providing certain observational evidence for the existence of helical magnetic fields in its inner jet regions.

Relativistic jet models (e.g., proposed in Qian 2019 and this work) can fully explain the emission properties from radio, infrared, optical through to γ-rays observed in OJ287 and a comprehensive and compatible framework has been tentatively constructed for interpreting the whole phenomena in blazar OJ287, which involve the following physical processes: (1) OJ287 may host a supermassive black hole binary with comparable masses for the primary and secondary holes in nearly co-planar eccentric orbital motion with an orbital period of $\sim$9 yr (in the source frame); (2) Both black holes may be spining (Kerr holes) and create their respective jets, directing toward the observer with

[7] Or shocks of spine-sheath structure as suggested in D'Arcangelo et al. (2009).

small viewing angles; (3) Cavity-accretion processes may occur in this black hole/disk system due to the interaction between the spinning black-holes, the circumbinary disk and the circumdisks, causing complex mass accretion events; (4) The eccentric orbital motion of the binary modulates the accretion flows onto the holes, resulting in the quasi-periodicity of the accretion events and consequential optical outbursts. The double-stream accretion flows during pericenter passages may result in the double structure of the quasi-periodic optical outbursts; (5) The accretion events created during the orbital motion would lead to the ejection of superluminal optical knots through jet-formation mechanisms, which emit at optical and radio wavelengths, including quasi-periodic outbursts and non-periodic intervening outbursts.

In brief, it may be possible to describe the chain of the physical processes as follows. The interaction between the binary holes and the circumbinary disk results in double-stream accretion flows (e.g., Tanaka 2013, Artymovicz 1998, Shi et al. 2012, D'Orazio et al. 2013) toward the binary holes during pericenter passages, creating superluminal optical knots ejected from the jets which produce the observed quasi-periodic outbursts with double-peak structure. During the remaining parts of the orbit the interaction between the holes and circumbinary disk also creates enhanced accretion events, causing the non-periodic outbursts. The optical outbursts consist of elementary flares, which are produced by a succession of individual superluminal optical knots due to lighthouse effect and blend together to form the complex outbursts.

If the relativistic jet scenario suggested in this work and Qian (2019) is correct, the optical phenomena in OJ287 coul be explained without needing to invoke the disk-impact mechanism and thermal impact-outbursts. However, the disk-impact mechanism looks very attractive for testing the effects of general relativity (Einstein 1916, 1918), if the claimed accurate timing of the primary quasi-periodic optical outbursts with uncertainty of $\sim$1 day is really confirmed in future.

In order to test the relativistic models, more observational and theoretical studies are needed. For finally clarifying the nature of optical radiation from the primary quasi-periodic outbursts (thermal or non-thermal), observations of γ-rays associated with the primary quasi-periodic optical outbursts are important. Complete information about the time-variable polarization (both polarization degree and polarization angle) of the primary quasi-periodic outbursts at multi-frequencies are needed. Model fittings are also needed to interpret the time-variable flux density curve I(ν, t), polarization degree curve p(ν, t) and polarization angle curve PA(ν,t). Generally, if the low polarization dip observed in polarization degree curves from the primary quasi-periodic flares is associated with the rapid change in its polarization angle, this quasi-periodic flare may be recognized as a synchrotron flare, originated from the relativistic jet (see Holmes et al. 1984). Observational studies of the correlation between variations in optical and radio frequencies on time-scales of $\sim$1 day will be very helpful, because radio variations simultaneous with the quasi-periodic optical outbursts will certainly imply the optical outbursts being non-thermal.

For the relativistic models currently available, an unresolved problem may be related to the timing of the primary quasi-periodic optical outbursts. In principle, cavity-accretion processes in comparable-mass and eccentric binary systems may provide some solutions to the quasi-periodicity and double-peak structure of the primary optical outbursts (Artymovicz 1998, Tanaka 2013, Shi et al. 2012, D'Orazio et al. 2013 and references therein). But theoretical model-simulations of the cavity accretion processes for specifically fitting the primary quasi-periodic optical outbursts and their double-structure pattern are required. Non-periodic optical outbursts should also be included. It seems that in relativistic jet models the quasi-periodic optical outbursts can not be accurately timed as required in the disk-impact model. In fact, for the optical outburst during 1995.8–1996.1 we can only recognize the large synchrotron outburst during JD2450050–2450105 (see Figure 3). The problem of outburst timing for OJ287 needs to be further investigated.

Acknowledgements. I wish to thank Dr. M. Aller (University of Michigan, USA) for affording the 14.5 and 8 GHz data on the optical outburst in 1995.84. I am most grateful to Dr. K. Nillson (Turku University Observatory, Finland) for providing the optical data during the OJ-94 project.

References

Ackermann M., Ajello M., Allafort A., et al., 2011, ApJ 743, 171
Agudo, I., Marscher, A.P., Jorstad, S.G., et al. 2012, ApJ, 747, 63
Allen, D.A., Ward, M.J., Hyland, A.R. 1982, MNRAS, 199, 969
Aller, M.D., Aller, H.D., Hughes, P.A. 1994, in: Workshop on Intensive Monitoring of OJ287, Tuorla Obs. Rep. Informo 174, ed. M.R. Kidger & L.O. Takalo (Turku: Univ. Turku), 60
Aller, M.F., Hughes, P.A., Aller, H.D. 2010, in "Fermi Meets Jansky - AGN in Radio and Gamma-rays", Eds.: Savolainen, T., Ros, E., Porcas, R.W. and Zensus, J.A., p65
Aller, M.F., Hughes, P.A., Aller, H.D., et al. 2014, ApJ, 791, 53
Artymowicz, P., Lubow, S.H. 1996, ApJ, 467, L77
Artymowicz, P. 1998, in: Theory of Black Hole Accretion Disks, ed. M.A. Abramowicz, G. Björnsson, J.E. Pringle, p202
Basta, M., Hudec, L. http://altamira.asu.cas.cz/iblwg/data/oj287, 2006
Beskin, V.C. 2010, Physics-Uspekhi, 53, 1199
Björnsson, C.I. 1982, ApJ, 260, 855
Björnsson, C.I. & Blumenthal, G.R. 1982, ApJ, 259, 802
Blandford, R.D., & Znajek, R.L. 1977, MNRAS, 179, 433
Blandford, R.D., Königl A., 1979, ApJ 232, 34
Blandford, R.D., & Payne, D.G. 1982, MNRAS, 199, 883
Britzen, S., Fendt, C., Witzel, G., Qian, S.J., et al. 2018, 478, 3199
Brown, L.M.J., Robson, E.I., Gear, W.K., Smith, M.G. 1989, ApJ, 340, 150
Camenzind, M. 1990, Reviews in Modern Astronomy, Vol.3, 234
Camenzind, M. & Krockenberger, M. 1992, A&A, 255, 59
Cohen, M.H. 2017, Galaxies, 5, 12
D'Arcangelo, F.D., Marscher, A.P., Jorstad, S.D., et al. 2009, ApJ, 697, 985
Dey, L., Valtonen, M.J., Gopakumar, A., et al. 2018, ApJ, 866, article id. 11D
Doeleman, S.S., Fish, V.L., Schenck, D.E., et al. 2012, Science, 338, 355
D'Orazio, D.L., Haiman, Z., & Macfadyen A. 2013, MNRAS, 436, 2997
Dreissigacker, O. 1996a, in: Extragalactic Radio Sources, eds., R. Ekers et al., p421
Dreissigacker, O & Camenzind, M. 1996b, in: Blazar Continuum Variability (ASP Conference Series, eds. H.R. Miller, J.R. Webb, and J.C. Noble), Vol.110, p.377
Einstein, A. 1916, Sitzungberichte der Königlich Presssichen Akademie der Wissenshafte (SPAW, Berlin), 688
Einstein, A. 1918, Sitzungberichte der Königlich Presssichen Akademi der Wissenshafte (SPAW, Berlin), 154
Gupta, A.C., Agarwal, A., Mishra, A., et al. 2016, MNRAS, 458, 1127
Hartman, R.C., Bertsch, D.L., Bloom, S.D., et al.1999, ApJS, 123, 79
Hayasaki, K., Mineshige, S. & Ho, L.C. 2008, ApJ, 682, 1134

Hodgson, J.A., Krichbaum, T.P., Marscher, A.P., et al. 2017, A&A, 597, 80
Hogg, D.W. 1999, astro-ph/9905116
Holmes, P.A., Brand, P.W.J.L., Impey, C.D.,et al. 1984, MNRAS, 211, 497
Kikuchi, S., Inoue, M., Mikami, Y., et al. 1988, A&A, 190, L8
Königl, A. & Choudhuri, A.R. 1985, ApJ, 289, 173
Komatsu, E., Dunkley, J., Nolta, M.R., et al. 2009, ApJS, 180, 330
Kushwaha, P., Gupta, A.C., Wiita, P.J., et al. 2018a, MNRAS, 473, 1145
Kushwaha, P., Gupta, A.C., Wiita, P.J., et al. 2018b, MNRAS, 479, 1672
Lehto, H.J., & Valtonen, M.J. 1996, ApJ, 460, 207
Li, Z.Y., Chiueh, T.H., Begelman, M.C. 1992, ApJ, 394, 459
Meier, D.L., Koide, S., Uchida, Y. 2001, Science, Vol.291, 84
Meier, D.L. 2013, EPJ Web of Conference 61, 01001
Neronov, A. & Vovk, Ie. 2011, MNRAS, 412, 1389
Qian, S.J., Witzel, A., Krichbaum, T.P., et al. 1991, Acta Astron. Sin., 32, 369 (english translation: in Chin. Astro. Astrophys., 16, 137 (1992))
Qian, S.J. 2013, Res. Astron. Astrophys., 13, 783
Qian, S.J. 2015, Res. Astron. Astrophy., 15, 687
Qian, S.J., Britzen, S., Witzel, A., et al. 2017, A&A, 604, A90
Qian, S.J. 2018, arXiv-1811.11514
Qian, S.J. 2019, arXiv-1904.03357
Schramm K.-J., Borgeest U., Camenzind M.,et al., 1993, A&A 278,391
Shi, J.M., Krolik, J.H., Loubow, S.H., Hawley J.F. 2012, ApJ, 749, 118
Sillanpää, A., Teerikorpi, P., Haarala, S., et al. 1985, A&A, 147, 67
Sillanpää, A., Haarala, S., Valtonen, M.J., et al. 1988, ApJ, 325, 628
Sillanpää, A., Takalo, L.O., Pursimo, T., et al. 1996a, A&A, 315, L13
Sillanpää, A., Takalo, L.O., Pursimo, T., et al. 1996b, ASP conference series, Vol. 110 (Blazar Continuum Variability), eds. H.R. Miller, J.R. Webb and J.C. Noble, p74
Spergel, D.N., Verde, L., Peiris, H.V., et al. 2003, ApJS, 148, 175
Sundelius, B., Wade, M., Lehto, H.J., et al. 1997, ApJ, 484, 180
Takalo, L.O. 1996a, ASP Conference Series, Vol.110 (Blazar Continuum Variability), eds., H.R. Miller, J.R. Webb and J.C. Noble, p70
Takalo, L.O., Sillanpää, A., Lehto, H.J. 1996b, Mem.S.A.It., 67, 545
Tanaka, T.L. 2013, MNRAS, 434, 2275
Tateyama, C.E., Kingham, K.A., Kayfmann, P., et al. 1999, ApJ, 520, 627
Usher, P.D. 1979, Astron. J., 84, 1253
Valtaoja, L., Sillanpää, A., & Valtaoja, E. 1987, A&A, 184, 57
Valtaoja, E., Terasranta, H., Tornikoski, M., et al. 2000, ApJ, 531, 744
Valtonen, M.J., Lehto, H.J., Sillanpää, A., et al. 2006, ApJ, 646, 36
Valtonen, M.J. 2007, ApJ, 659, 1074
Valtonen, M.J. & Ciprini, S. 2012, Mem.S.A.It., 83, 219
Valtonen, M.J., Dey, L., Hudec, R., et al. 2018, in: Gravitational Waves Astrophysics: Early Results from Gravitational Wave Searches and Electromagnetic Counterparts, Proceedings of IAU Symposium, Vol. 338, p29
Valtonen, M.L., Zola, S., Jermak, H., et al. 2017, Galaxies, 5, 83
Villata, M., Raiteri, C.M., Sillanpää, A., et al. 1998, MNRAS 293, L13
Villforth, C., Nilsson, K., Heidt, J., et al. 2010, MNRAS 402, 2087
Vlahakis, N., & Königl, A. 2004, ApJ, 605, 656
Wagner S.J., Camenzind M., Dreissigacker O., et al., 1995, A&A 298, 688